Proceedings of OMAE2005
24th International Conference on Offshore Mechanics and Arctic Engineering (OMAE 2005)
June 12-17, 2005, Halkidiki, Greece

OMAE2005-67311

WATER ENTRY AND EXIT OF A HORIZONTAL CIRCULAR CYLINDER

Xinying Zhu
Department of Marine Technology, Norwegian University of Science and Technology, Trondheim, Norway
Email: xinying@ntnu.no

Odd M. Faltinsen
Centre for Ships and Ocean Structures, Norwegian University of Science and Technology, Trondheim, Norway

Changhong Hu
Research Institute for Applied Mechanics, Kyushu University, Fukuoka, Japan

ABSTRACT

This paper describes the fully nonlinear free-surface deformations of initially calm water caused by water-entry and water-exit of a horizontal circular cylinder with both forced and free vertical motions. This has relevance for marine operations as well as for the ability to predict large amplitude motions of floating sea structures. A new numerical method called the CIP (Constrained Interpolation Profile) method is used to solve the problem.

In this paper, the circular cylinder and free surface interaction is treated as a multiphase problem, which has liquid (water), gas (air) and solid (circular cylinder) phases. The flow is represented by one set of governing equations, which are solved numerically on a non-uniform, staggered Cartesian grid by a finite difference method. The free surface as well as the body boundary is immersed in the computational domain.

The numerical results of the water entry and exit force, the free surface deformation and the vertical motion of the cylinder are compared with experimental results, and favorable agreement is obtained.

INTRODUCTION

The Boundary Element Method (BEM) has been successful in solving linear and second-order wave-body interaction problems that can be described by potential flow theory. Good results have also been demonstrated for strongly nonlinear and violent fluid motion. An example is the water entry study by Zhao & Faltinsen (1993). However, the method fails for instance when a plunging wave impacts on the underlying water. Moyo & Greenhow (2000) studied by BEM the fully non-linear inviscid-flow calculations of the deformations of an initially calm free surface caused by the free motion of a horizontal cylinder starting from rest from a prescribed depth. The calculations break down when the cylinder is almost totally above the initial free surface with a thin layer of fluid riding on its upper surface and two (symmetric) regions of negative pressure on its lower surface. The resulting pressure inversion across the free surface immediately below the cylinder causes Rayleigh-Taylor instability and spontaneous free surface breaking of the type photographed by Greenhow & Lin (1983) . This stops the numerical calculations.

CFD methods based on solving the Navier-Stokes equations are generally more robust than the BEM to solve violent fluid motion. Mixture between air and fluid may occur and viscous effects can matter. However, the accuracy of a CFD method for different applications such as sloshing in tanks, green water on deck, slamming and large amplitude ship motions have to be documented. Important verification and validation tests of a CFD method are also how well it can predict linear fluid problems. CFD methods are still too time-consuming for practical strongly nonlinear 3D wave-ship interaction problems. Long time simulations are then needed in order to obtain probability density functions of response variables in a stochastic sea.

Both grid methods and gridless methods are used to solve the Navier-Stokes equations. The Smoothed Particle Hydrodynamics (SPH) method is an example on a gridless method. The Volume of Fluid (VOF) method, the Level Set (LS) method and the Constrained Interpolation Profile (CIP) method use an Eulerian grid.

We are in this paper using the CIP-based finite difference method described by Hu & Kashiwagi (2004) to study two-dimensional water entry and exit of a circular cross-section. This has relevance for wave loads on a horizontal member of a

jacket structure in the splash zone, marine operations where units are lowered from a crane ship through the free surface and large amplitude wave-induced motions and loads on floating structures.

The water exit has been far less studied than the water entry. The water entry phase includes the slamming, i.e. the impact between the body and the free surface. This can be associated with the formation of air pockets and local hydroelastic effects. We include the air flow, but assume a rigid structure. The compressibility of the water matters only in a very small initial time and is not believed important for the structural response. Gravity and viscosity do not matter in the initial water entry phase. However, both these two effects must be considered at a later stage of the water entry and during the water exit phase. Viscous effects become important when viscous flow separation occurs. The latter requires the existence of points on the cylinder surface where the shear stress is zero. This takes time to develop after the start up flow around the cylinder. This has been discussed by Schlichting (1979) for the flow around a circular cylinder in infinite fluid. There occurs Froude number dependent non-viscous flow separation from the cylinder surface during the penetration of the cylinder in our studied water entry cases. An open air cavity is then formed above the cylinder. The non-viscous flow separation is important for the hydrodynamic loads on the cylinder.

We will in the main text compare the CIP-based method by existing experimental results for forces and motions during the entry and exit phase. The initial impact and the non-viscous flow separation represent numerically the most difficult phases of the water entry. The final water exit phase before penetration of the cylinder is also numerically challenging.

NUMERICAL METHOD

The CIP-based finite difference method used in this study is described in detail by Hu & Kashiwagi (2004). Two-dimensional water and air flow in interaction with a solid body is considered. The fluid is assumed compressible and viscous. Temperature variations are neglected. The governing equations for the fluid are

$$\frac{\partial \rho}{\partial t} + u_i \frac{\partial \rho}{\partial x_i} = -\rho \frac{\partial u_i}{\partial x_i} \qquad (1)$$

$$\frac{\partial u_i}{\partial t} + u_j \frac{\partial u_i}{\partial x_j} = -\frac{1}{\rho}\frac{\partial \sigma_{ij}}{\partial x_j} + f_i \qquad (2)$$

$$p = f(\rho) \qquad (3)$$

where:
t is the time variable;
x_i (i =1,2) are the coordinates of a Cartesian coordinate system;
ρ is the mass density;
u_i (i=1,2) are the velocity components;
f_i (i=1,2) are due to the gravity force.

Further, σ_{ij} is the total stress and is expressed as

$$\sigma_{ij} = -p\delta_{ij} + 2\mu (1-\delta_{ij}/3) S_{ij}$$

where

p is the pressure;
μ is the dynamic viscosity coefficient;
δ_{ij} is the Kronecker's delta function;

$$S_{ij} = \frac{1}{2}\left(\frac{\partial u_i}{\partial x_j} + \frac{\partial u_j}{\partial x_i} \right)$$

The expression for σ_{ij} implies a modeling of the bulk viscosity for compressible fluid that can be questioned; see White (1974). If turbulent flow is considered, the equations have to be averaged over the time scale of turbulence and additional equations describing the Reynolds stresses must be introduced. We assume laminar flow in the following studies. This is appropriate for the boundary layer flow in the considered Reynolds number range. Even though the boundary layer flow is laminar and flow separation occurs, the separated flow will be turbulent for the considered Reynolds numbers. However, it is more important to correctly predict the boundary layer flow and where flow separation occurs than the fact that the separated flow is turbulent.

The equation of state given by Eq. (3) can be rewritten by Eq. (1). This gives

$$\frac{\partial p}{\partial t} + u_i \frac{\partial p}{\partial x_i} = -\rho C^2 \frac{\partial u_i}{\partial x_i} \qquad (4)$$

where $C = \sqrt{dp/d\rho}$ is the sound speed.

Density functions φ_m (m=1,2,3) are introduced to identify which part is the air, the water or the solid body. We use that $\varphi_1 = 1$ for the water and zero for the air and the body, $\varphi_2 = 1$ for the air and zero for the water and the body while $\varphi_3 = 1$ for the body and zero for the water and the air. These functions satisfy

$$\frac{\partial \varphi_m}{\partial t} + u_i \frac{\partial \varphi_m}{\partial x_i} = 0 \qquad (5)$$

The numerical method causes no sharp interface between air and water, i.e., the values of φ_1 and φ_2 change continuously between the values for air and water at the free surface. The same happens with the density functions between the body and the air and the water.

The CIP-based method uses also information about the spatial derivatives $\partial/\partial x_i$ of ρ, u_i, p and φ_m. Equations are obtained by differentiating Eqs. (1), (2), (4) and (5) with respect to x_i.

A time-independent rectangular grid covering the air, water and solid body is used. The flow variables are found as a function of time at the grid points. A constraint within each computational cell is that $\sum_{m=1}^{3} \varphi_m = 1$. The time integration of the equations is based on an Euler method and a fractional step method consisting of three steps. The first step is called the advection phase. It means that the right hand sides of Eqs.(1), (2), (4) and (5) and the spatial derivatives of these equations are set equal to zero. The equations have the mathematical form

$$\frac{\partial \chi}{\partial t} + u_i \frac{\partial \chi}{\partial x_i} = 0 \qquad (6)$$

When finding intermediate artificial values of the response variables χ at a grid point (k,l) at time step n+1 in the advection phase, we consider the upstream cell of the grid point. A third order polynomial expresses the variation of ρ, u_i, p and φ_m in the upstream cell at time step n in term of its values and spatial derivatives at (k,l) and the three other corner points of the cell. We can then easily express the χ at (k,l) at time step n+1 by means of a semi-Lagrangian method. There are two non-advection phases in the fractional step approach using the Euler method. One of them involves solving a Poisson equation for the pressure at time step n+1. The latter part is the most time consuming.

RESULTS AND DISCUSSIONS

In this section, the classical problems of water-entry and water-exit of a horizontal circular cylinder are solved by using the CIP-based method presented above. The results are compared with model tests.

Convergence studies

A horizontal circular cylinder is forced through an initially calm water surface with a constant vertical velocity V. The submergence of the lowest point on the cylinder relative to the calm water surface is h=Vt. Here t is the time variable with t=0 corresponding to the initial time of impact. The slamming coefficient Cs is defined as

$$Cs \equiv \frac{F_3}{\frac{1}{2}\rho V^2 2R} \qquad (7)$$

Here ρ is the mass density of water; R is the radius of the circular cylinder; F_3 is the total vertical hydrodynamic force resulting from the water entry, including the buoyancy force. The viscosity causes a shear force and influences the pressure loads. The effect of viscosity matters for the hydrodynamic force when viscous flow separation occurs. The dominant effect is due to the influence on the pressure loads. However, we cannot separate out what is the influence of viscosity and potential flow effects.

Figure 1 shows how the slamming coefficient Cs as a function of submergence depends on the time step size dt. From this figure, no convergence is apparent at the early stage of the impact. The difficulty in solving this problem can be understood from the numerical results by Zhao & Faltinsen (1993) for water entry of wedges with constant velocity. A non-viscous and incompressible fluid was assumed and a Boundary Element Method (BEM) was applied. The air flow and gravity were neglected. The smaller the deadrise angle β was, the more difficult it was to obtain convergent results. The lowest examined β was 4°. The local deadrise angle is initially zero during the water entry of a circular cylinder. We are better off during the initial impact with using the analytical Wagner's (1932) solution, which shows that the time rate of change of the wetted area 2c in the outer flow domain is proportional to $1/\sqrt{t}$, i.e. the solution is singular at t=0. The outer flow domain excludes the detailed flow in the spray roots and the jets causing spray. The numerical time integration method ought to recognize this singular behavior and an Euler method is inadequate. The Wagner method gives that $Cs=2\pi$ at t=0.

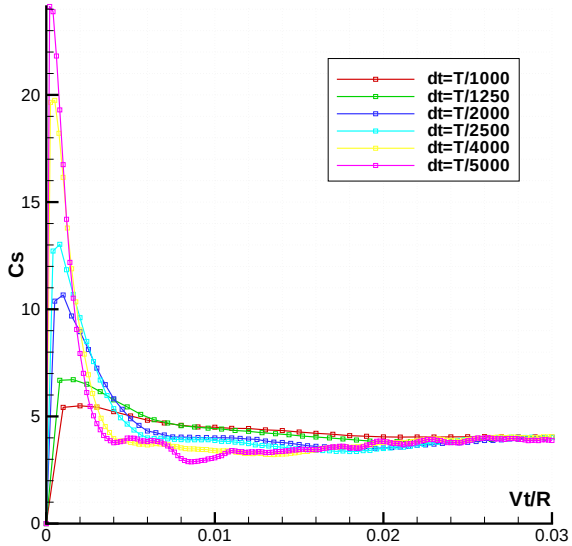

Fig. 1 Slamming coefficient Cs as a function of non-dimensional submergence Vt/R. Here: dt is the time step size used in the numerical integration; T=R/V where R is cylinder radius and V is water entry velocity. The calculations are for the test condition No. 1 in Miao's (1989) experiments (see Table 1)

The effect of compressibility and air flow will influence the results. However, it is believed that the origin of our numerical difficulties illustrated in Fig. 1 is associated with the very rapid initial change of the wetted surface. Although we cannot get convergence of F_3 at the early stage of impact, we can see that all the curves in Fig. 1 converge after a small submergence $Vt/R \approx 0.02$. However, for some problems, what is important for the global response of the structure during a small time increment Δt after the impact is the force impulse rather than the instantaneous value of the force. The force impulse is defined as

$$I = \int_0^{\Delta t} F_3(t)dt \qquad (8)$$

We compared therefore time-averaged Cs-values (related to the force impulse I) during the small submergences (related to small time increment Δt) Vt/R=0~0.02 and Vt/R=0~0.03 as a function of the time step size. From Fig. 2, convergence for the averaged Cs can be obtained when a small time step size is used.

The initial impact phase results by using the time-averaged Cs are in reasonable agreement with the empirical formulas by Miao (1989) and Campbell & Weynberg (1980). We will now investigate the numerical results for a broader range of Vt/R.

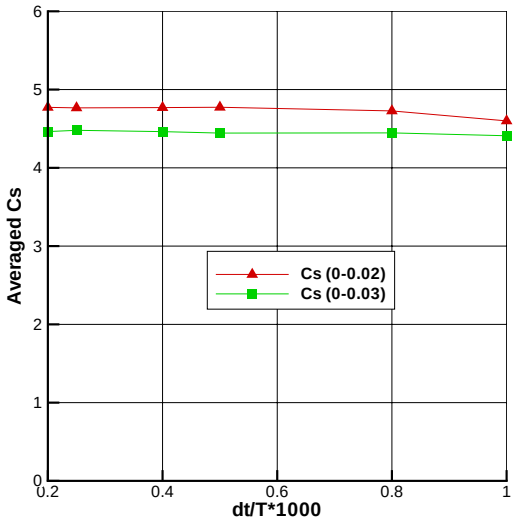

Fig. 2 Averaged initial slamming coefficient Cs as a function of non-dimensional time step size dt/T. Here Cs (0-0.02) denotes the slamming coefficient averaged from Vt/R=0 to 0.02; Cs (0-0.03) is the slamming coefficient averaged from Vt/R=0 to 0.03.

Water entry with constant velocity

Our CIP method will be compared with the water entry tests by Miao (1989) in the No. 2 tank at the Marine Technology Centre in Trondheim. The basin is 28m long, 2.5m wide and has a water depth of 1.0m. A test cylinder with diameter D=0.125m and length L=0.25m was used in measuring the impact forces. In order to achieve a two-dimensional flow condition, the model was equipped with two rectangular stiffened end plates with height H=0.4m and width B=0.3m. A hydraulic system drove the model vertically downwards. The stroke was regulated by an electronically operated valve in combination with the measurements of the position of the test cylinder by means of a potentiometer. The water entry velocity was determined from an average slope computed from the position data. Other parameters for the water entry tests are shown in Table 1.

Table 1 Parameters for the water entry tests by Miao (1989)

Test No.	No.1	No.2	No.3	No.4	No.5
V(m/s)	0.5124	0.639	0.760	0.876	1.024
F_n	0.4627	0.577	0.6863	0.791	0.9247

The numerical grid is rectangular with horizontal and vertical lengths Δx and Δy (see Fig. 3) that vary in the computational domain. The smallest values are used at the cylinder. The minimum non-dimensional lengths are $\Delta x/R=0.02$ and $\Delta y/R=0.02$. The computational domain has a breadth and height of 400R and 50R, respectively. The total number of cells is 500×435.

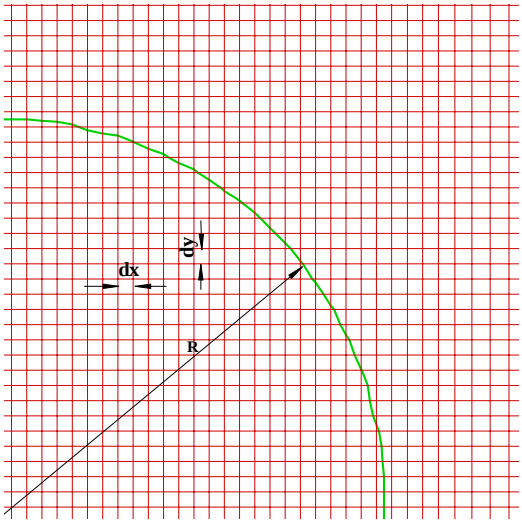

Fig. 3 Grid distribution of part of the circular cross-section with radius R and its close vicinity.

The non-dimensional impact force defined by Eq. (7) can be expressed as

$$Cs = f(\frac{Vt}{D}, F_n, Re, ...)$$

where $F_n = V/\sqrt{gD}$ is the Froude number, Re=VD/ν is the Reynolds number and $\nu = \mu/\rho$ is the kinematic viscosity of water. Other possible parameters influencing Cs are the roughness number k/D, the Weber, cavitation and Cauchy numbers. Here k is the mean height of the roughness on the cylinder surface.

The viscous parameters k/D and Re will matter for the force magnitude after viscous flow separation has occurred. This will in practice for water entry mean that the whole cylinder surface is wetted and the cylinder has penetrated many cylinder radii. The cavitation number must be considered if air cushions are formed. The Weber and Cauchy numbers account for the surface tension and the compressibility of the water, respectively. The compressibility of the water matters at a very small initial time, when the speed of sound in water is smaller or the order of $\sqrt{VR/t}$. The latter is the theoretical velocity of half of the wetted surface at an initial stage when the effects of air cushion, air flow and free surface deformation are neglected. Let us exemplify what this time scale means by setting the speed of sound, i.e. $1400 ms^{-1}$, equal to $\sqrt{VR/t}$ and use $V=0.5124 ms^{-1}$ together with R=0.0625m. This gives the time $1.634\cdot 10^{-8}$ s or $Vt/R = 1.34\cdot 10^{-7}$. This corresponds to a significantly smaller time than the time steps used in the calculations presented in Fig. 1. The consequence is that we have not properly modeled the effect of the compressibility in the water.

Our further discussion will focus on the influence of Vt/D, F_n and Re. A smooth cylinder surface is assumed. The Froude number dependence is both due to the free surface wave generation and the buoyancy force.

In order to check the influence of Reynolds number on Cs, both a low and a high Reynolds number in the subcritical flow regime are used in the calculations and the comparisons are shown in Fig. 4, Fig. 5 and Fig. 8. The Reynolds number was obtained by varying fictitiously the kinematic viscosity of water. The results show a small difference between the high and low Reynolds numbers. This is an expected result for this Reynolds number variation in the subcritical flow regime. The vorticity in the fluid was calculated in order to assess the influence of the viscous forces. Since the major vorticity was concentrated in the boundary layer of the cylinder, there is a small effect of viscosity on the pressure. Further, the frictional force gave a very small contribution to the total force.

We can explain qualitatively the behavior of Cs as a function of Vt/R by expressing the total vertical force as $F_3 = VdA_{33}(t)/dt + \rho gA(t)$. Here A_{33} is the 2D infinite-frequency heave added mass and A(t) is the cylinder area below the mean free surface; see Faltinsen (1990). $dA_{33}(t)/dt$ is largest at t=0 and decreases with increasing Vt/R while A(t) increases with time. The combination of $VdA_{33}(t)/dt$ and $\rho gA(t)$ causes a minimum Cs as we see occurs at about Vt/R=0.5 in the examined cases. This approach does not account for the fact that the water separates from the cylinder and causes an open air cavity above the cylinder. It follows by continuity of fluid mass that the water displaced by the cylinder and the air cavity causes an increased water elevation. This free surface wave generation affects the vertical force. A large part of the force at the final stage when the cylinder surface is totally wetted is due to the buoyancy.

If the cylinder is totally submerged, the contribution of the buoyancy to the slamming coefficient is

$$C_{Sb} = \frac{\rho g \pi D^2/4}{\frac{1}{2}\rho V^2 D} = \frac{\pi}{2}\frac{1}{F_n^2} \qquad (9)$$

This value is presented in Fig. 4 -Fig. 8 from the time when the cylinder is totally submerged. As one can see from these figures, the time for being totally wetted increases with increasing water entry velocity. There is a maximum in Cs a small time before the cylinder is totally submerged.

From Fig. 4 - Fig. 8, some differences exist between the numerical results and the experimental data at the final stage of impact. The fact that we predict correctly the buoyancy force for the totally submerged phase is no surprise. So, in order to judge the accuracy of the predictions, we must deduct the buoyancy force. This increases the errors in the numerical predictions relative to the experiments. However, the experiments have errors as well. Experimental error sources could be

- Buoyancy force due to the stiffened end plates. This contribution to the slamming coefficient is approximately 0.03 at Vt/R=0 and is about 0.1 after Vt/R=4.2.
- 3D flow effects in the experiments. Although the two end plates were used on the model cylinder, it is impossible to completely get rid of 3D effects and to achieve 2D flow. This was numerically documented in the present case by evaluating the 2D flow velocity around the cylinder at the position of the plate edges. Since this was not negligible, we anticipate some 3D flow effects. We cannot quantify this. However, we expect that the 2D flow assumption represent a good approximation.
- Cross flow with flow separation at the edges of the end plates as a consequence of 3D flow.
- Frictional force on the end plates. The vertical frictional force on the end plates can be estimated by $F = \frac{1}{2}\rho C_F V^2 S$, where S is the area of both sides of the two end plates, i.e. S=4HB. C_F is approximated by $C_F = 0.075/(\log_{10}Re-2)^2$, where Re=VH/ν. The contribution of the frictional force to the slamming coefficient is $C_{SF} = F/(\frac{1}{2}\rho V^2 DL)$, which is approximately equal to 0.01. One should note that the estimation assuming totally wetted plate sides is an approximation. Further, the effects of stiffeners and the fact that the velocity along the inside of the plates is spatially varying due to the presence of the cylinder are ignored. However, our objective is to estimate qualitatively the contribution of frictional force to the slamming coefficient. We find that this contribution is about 0.01, i.e. it is negligible.
- Possible root vortices at the intersection lines between the plates and the cylinder. We cannot estimate this effect.
- Natural frequencies of the test rig, including possible hydroelastic effects. Chezhian (2003) documented clear hydroelastic effects in his experimental drop tests of a horizontal 3D structure with circular cross-sections. The oscillatory nature of the experimental slamming coefficient suggests either hydroelastic effects, eigenfrequency oscillations of the test rig, or air cavity oscillations. Miao (1989) said without giving detailed explanations that the 140Hz oscillations seen in the experiments can be associated with the measuring system. However, oscillations with smaller frequencies occur also in the force measurements, in particular when the cylinder surface is totally wetted. We made a rough estimate of the possibility of oscillations of air bubbles. This was done by guessing the possible dimensions of the air bubbles and estimating the natural frequency of the air bubble oscillations; see Faltinsen (2005). We found that this could not explain the oscillating behavior of Cs.

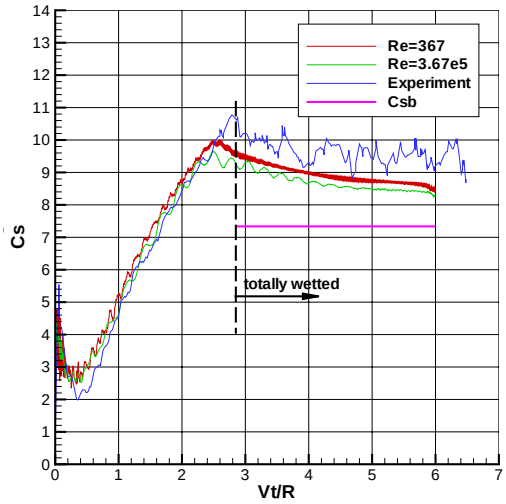

Fig. 4 Slamming coefficient Cs as a function of Vt/R for the water entry test No. 1

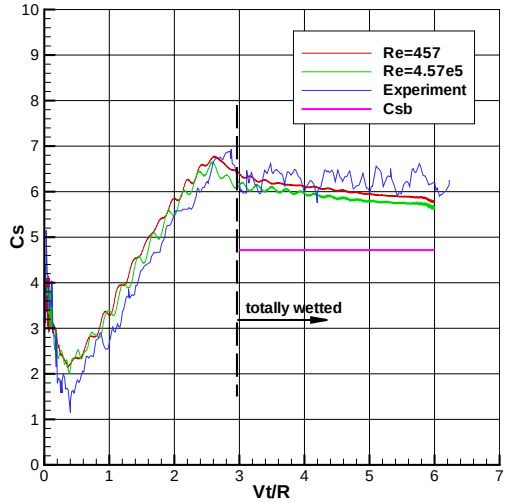

Fig. 5 Slamming coefficient Cs as a function of Vt/R for the water entry test No. 2

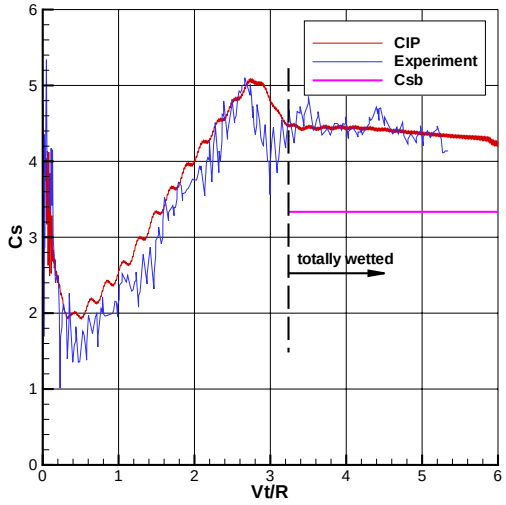

Fig. 6 Slamming coefficient Cs as a function of Vt/R for the water entry test No. 3

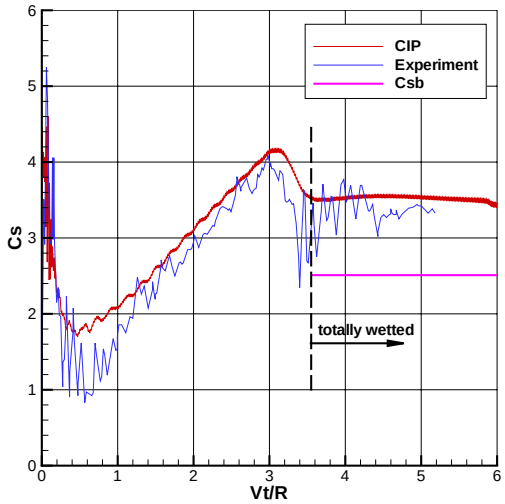

Fig. 7 Slamming coefficient Cs as a function of Vt/R for the water entry test No. 4

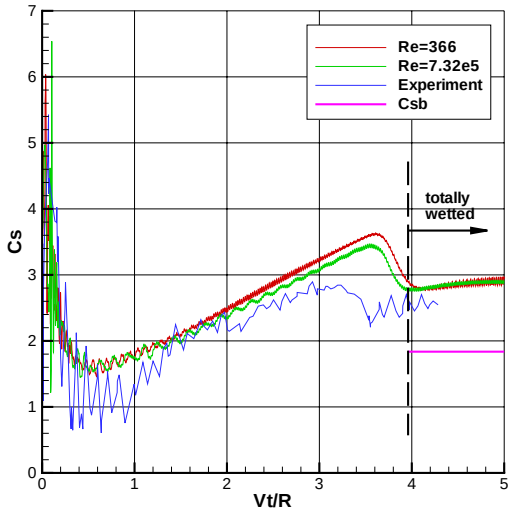

Fig. 8 Slamming coefficient Cs as a function of Vt/R for the water entry No. 5

Water exit with constant velocity

Similarly as for the water entry studies, the grid used in the water exit calculations is also rectangular. The smallest horizontal and vertical lengths are used at the cylinder. The minimum values are $\Delta x/R=0.04$ and $\Delta y/R=0.04$. Other parameters for the water exit tests are shown in Table 2.

Table 2 Parameters for the water exit tests by Miao (1989)

Test No.	No.1	No.2
V(m/s)	0.5124	0.7644
F_n	0.4627	0.6903

Some minor corrections were made with the experimental data to make it possible to compare with the numerical results. Buoyancy force due to the stiffened end plates has been subtracted from the experimental data. Its contribution to the vertical force matters until Vt/R=4.2, where t=0 corresponds to

the time when the top of the cylinder reaches the mean free surface.

Figure 9 and 10 present comparisons of the exit coefficient Ce between the CIP calculations and the experiments by Miao (1989). Here Ce is defined in the same way as the slamming coefficient Cs; see Eq. (7). The overall agreement is good. The cylinder was initially at rest at Vt/R=-5.5, and was accelerated harmonically to a constant velocity V at Vt/R=-5 in the numerical simulations. We note large oscillations in the experimental force. This is believed to be experimental errors associated with unwanted vibrations of the test rig causing added mass and structural inertia forces on the test cylinder. The vibrations are probably connected with the automatic control of the hydraulic system used to force the test cylinder out of the water. The control system was based on the position measurements. However, small deviations in the position can cause large accelerations. Let us illustrate this by an example based on the data in Fig. 10. There is from Vt/R=-4.5 to -3.2 a large amplitude oscillation of Ce which we denote as Ce_0. We use a harmonic approximation, i.e. $Ce_0 \sim C_a \sin(\omega t+\alpha)$, where ω is estimated as 60(rad/s). We neglect the structural mass and approximate the oscillatory force amplitude as $\rho\pi R^2\omega^2 A$, where A is the amplitude of the oscillations of the test rig. Using the definition of Ce and estimating the amplitude C_a of the oscillatory part Ce_0 of Ce as 2.4 gives A/R=0.03, i.e. A is a small value as we anticipated. The velocity amplitude ωA associated with this oscillatory behavior is 0.11V. We note that the oscillatory forces are largest at the start-up. Similar behavior was also seen during the water entry tests at the start-up of the cylinder above the mean free surface. This confirms our suspicion that the oscillatory forces are due to the transient effects of the hydraulic system.

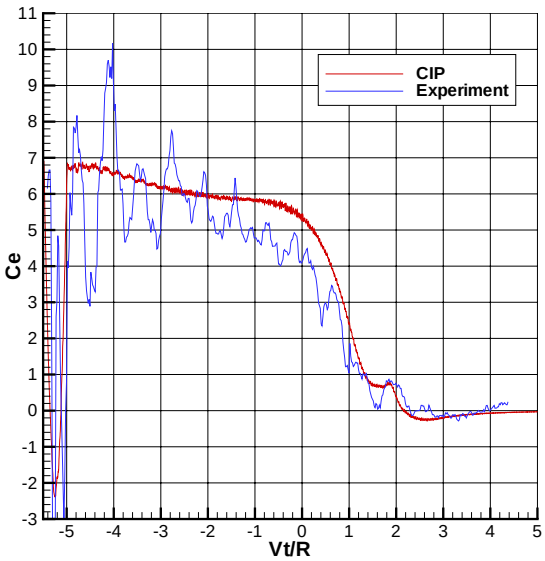

Fig. 9 Exit coefficient Ce as a function of Vt/R for the water exit test No. 1

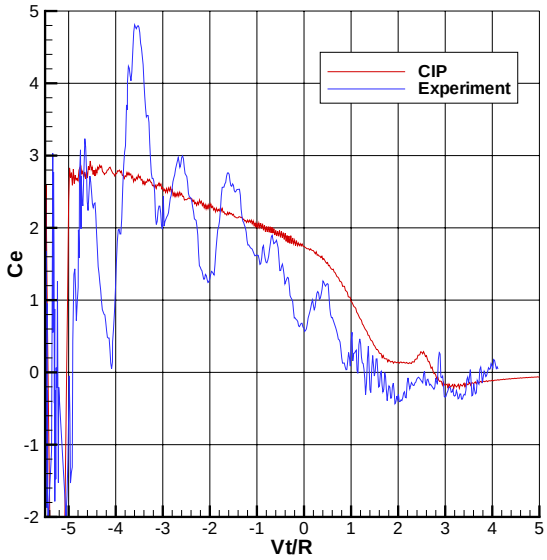

Fig. 10 Exit coefficient Ce as a function of Vt/R for the water exit test No. 2

In order to further explain physically the results, we will introduce a simplified model that accounts for buoyancy, viscous drag and a potential flow force expressing the time rate of change of heave added mass. This model does not account for the deformation of the free surface which is important when the cylinder is close to the free surface. We believe that a rigid wall condition is a proper free surface condition for the exit problem when the cylinder is not too close to the free surface.

It follows by the time rate of change of the kinetic fluid energy, the "rigid-wall" free surface condition and potential flow theory that there is a vertical hydrodynamic force $F=0.5VdA_{33}(t)/dt+A_{33}dV/dt$ acting on the cylinder. We notice that the structure of this expression differs from the force expression $d(A_{33}V)/dt$ used in the simplified water entry calculations. The reason is the difference in the free surface conditions. For constant exit velocity, $F=0.5V^2dA_{33}/dz$. Here z=0 is the mean free surface and the vertical z-coordinate is positive downwards. F is positive upwards. The 2D heave added mass A_{33} for the circular cylinder satisfying the rigid-wall condition is estimated by generalizing the asymptotic formula for large z/R by Sun (2004), i.e.

$$\frac{A_{33}(z)}{\rho\pi R^2} = \frac{\alpha^4 - 1}{\alpha^4 - 2\alpha^2} \qquad (10)$$

where $\alpha = 2p/R$ and z=p means the z-coordinate of the cylinder axis. This agrees well even for small (p/R-1) with the asymptotic expression for small (p/R-1) by Walton (1986). Since Walton's formula is not good for large (p/R-1), we have used Eq. (10) in our calculations even though it is not exact for very small (p/R-1). Since our objective is only to show the trend in the force for small (p/R-1), this is sufficient. The free surface will in reality not be a wall when the cylinder is close to the free surface.

The viscous drag coefficient was estimated by curve-fitting the experimental data by Sarpkaya (1966) as

$$C_D = p_1 t^{*5} + p_2 t^{*4} + p_3 t^{*3} + p_4 t^{*2} + p_5 t^{*} + p_6 \qquad (11)$$

Here $t^{*} = Vt'/R - 0.351 \geq 0$ and the time $t' = 0$ is the start of the flow. The non-dimensional p_i-coefficients are given as follows $p_1 = 2.4805 \cdot 10^{-7}$, $p_2 = -3.647 \cdot 10^{-5}$, $p_3 = 1.9058 \cdot 10^{-3}$, $p_4 = -4.4173 \cdot 10^{-2}$, $p_5 = 4.3146 \cdot 10^{-1}$, $p_6 = 7.3386 \cdot 10^{-2}$.

When $0 \leq Vt'/R \leq 0.351$, C_D equals to zero. These results are for subcritical flow, i.e. the boundary layer flow is laminar. This is appropriate for the model tests. However, the boundary layer flow upstream of the separation points on the cylinder surface may be turbulent in full scale conditions. This has an important effect on C_D. Further, Sarpkaya's results are for an infinite fluid and nearly constant velocity V. Both the presence of the free surface and the time variation of V will influence C_D.

Then, the total vertical hydrodynamic force including the contributions due to the buoyancy force is expressed as follows:

$$F_3 = \rho g \pi R^2 - 1/2 \rho C_D D V^2 + 0.5 V^2 dA_{33}/dz \qquad (12)$$

Figure 11 shows the calculations with this simple formula. It demonstrates that the buoyancy and viscous forces dominate when $Vt/R \leq -1$. When $-1 < Vt/R \leq 0$, there is a dominant effect due to the time rate of change of the kinetic fluid energy.

Figure 12 shows the comparisons between the simplified formula and the CIP calculations. It demonstrates a good agreement when $Vt/R \leq -1$. This means implicitly that the CIP calculations are consistent with Sarpkaya's experiments for the time variation of the viscous drag coefficient. A major effect of the viscous force is due to viscous flow separation. This can implicitly be seen from Fig. 13 which shows numerically predicted vorticity in the fluid and demonstrates that the vorticity is not concentrated in the boundary layer along the cylinder as it was for our water entry studies. The agreement between the simplified formula and the CIP calculations is not good for $-1 < Vt/R \leq 0$. However, since a significant deformation of the free surface occurs then, this should not be expected. The time dependent free surface elevation is illustrated in Fig. 14, by showing the density function φ_1 which is theoretically one for water and zero for the body and the air. Red and blue colors mean one and zero, respectively. The presence of other colors is caused by numerical errors and illustrates that the interfaces between the water and the air and the body are not sharp in the numerical simulations.

However, returning now to Fig. 9 and 10, we then see both in the experiments and in the CIP calculations that a significant change in the vertical force occurs when the cylinder is close to the free surface. We can, based on the calculations with the simplified formula, say that this rapid change in force is in a qualitative way associated with the large rate of change of the kinetic fluid energy. We believe that at the final stage of the water exit when the total force becomes close to zero, ventilation in the fluid below the cylinder and above the mean free surface occurs. This will be made evident later in the text.

The numerical results for Vt/R<-1 should be compared with the experimental data obtained after filtering out the oscillatory force behavior. We explained the oscillations earlier as an experimental error due to the hydraulic system. The averaged experimental data are in fair agreement with the numerical simulations. However, the oscillations of the cylinder will influence the time development of the drag coefficient through changes in the time history of the separation points. This will require further studies.

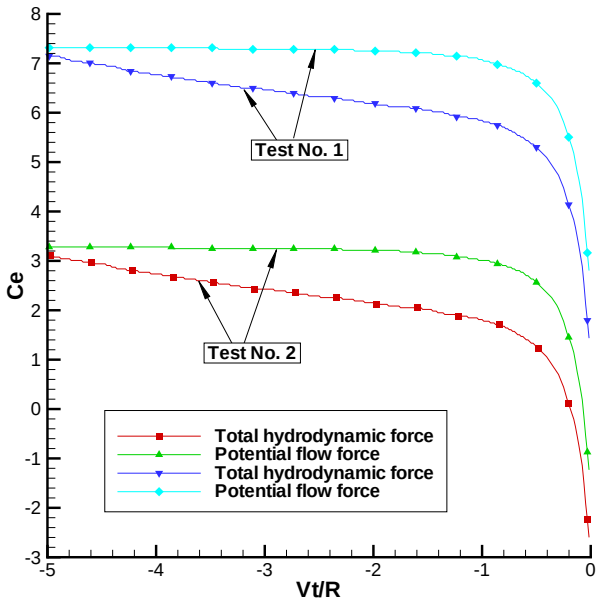

Fig. 11 Simplified calculations of the exit coefficient $Ce=F_3/(0.5\rho V^2 2R)$ by Eq. (12) with and without the effect of viscous drag force as a function of Vt/R for the two water exit tests.

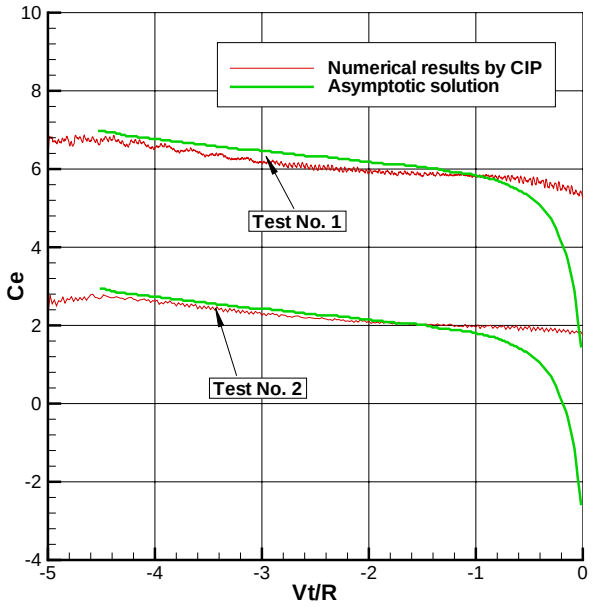

Fig. 12 Comparisons between the simplified formula (Eq. (12)) and the CIP calculations for the two water exit tests. $Ce=F_3/(0.5\rho V^2 2R)$

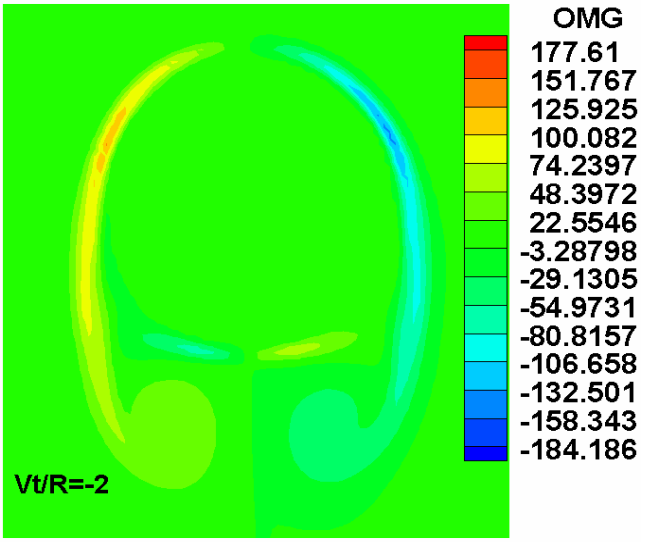

Fig. 13 Numerically predicted vorticity field for the water exit test No. 1. OMG means the vorticity with dimension s^{-1}

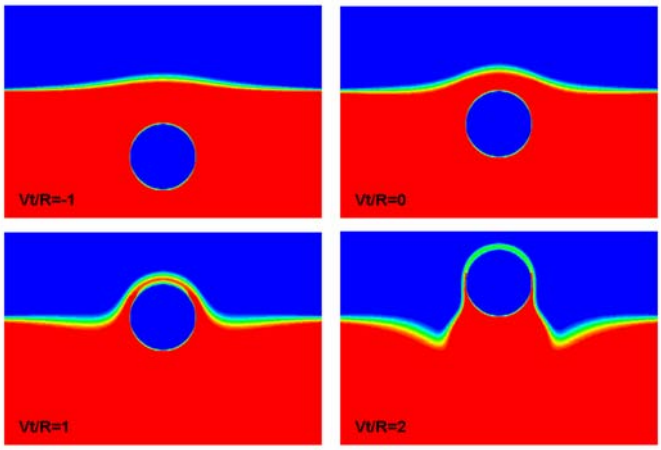

Fig. 14 Visualization of free surface deformation for the water exit test No. 2. The pictures present the density function φ_1 which is theoretically one for water and zero for the body and the air. Red=1. Blue=0.

Water entry with free motion

Now we consider the free surface profiles caused by a circular cylinder dropped into calm water. A half-buoyant and a neutrally buoyant circular cylinder with a radius of 5.5cm are used in the calculations. The depth of water is 0.30m. The cylinder was dropped from a height of 0.5m between the lowest point of the cylinder and the mean free surface. Numerical results are compared with the experiments conducted by Greenhow & Lin (1983).

Figure 15 shows the free surface deformation of a half-buoyant cylinder. As one can see, after the cylinder reaches the free surface, two jets are thrown up on both sides of the cylinder and move away from the cylinder, leaving the upper part of the cylinder dry even when h/R>2, where h is the submergence of the lowest point on the cylinder relative to the mean free surface. The non-viscous flow separation from the cylinder is by no means trivial to numerically predict. The authors are aware of other CFD methods having difficulties with this. Obviously the prediction of the non-viscous flow separation can be influenced by the grid size. Relatively small grids were used at the areas of flow separation in our numerical simulations.

Figure 16 shows the depth of penetration of the cylinder. Fairly good agreements can be obtained between the numerical results and experimental data for a half-buoyant cylinder.

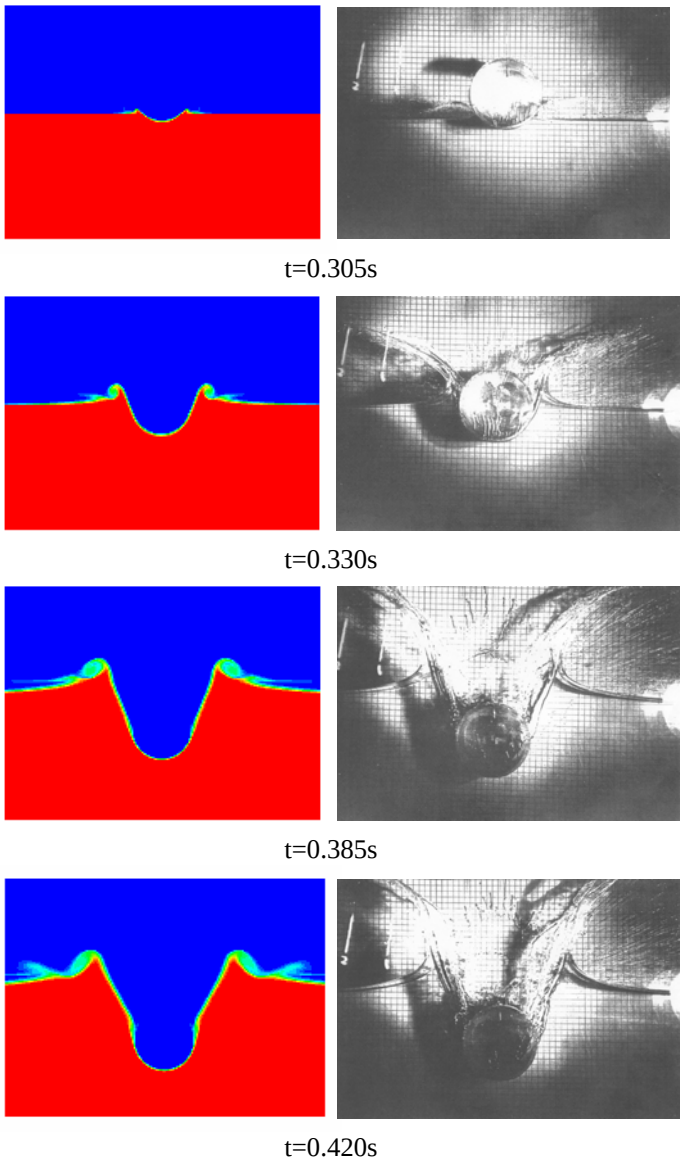

Fig. 15 Free surface deformation during water entry of a half-buoyant cylinder. CIP simulations (left) and experiments by Greenhow & Lin (right). The CIP calculations show the density function φ_1 which is theoretically one for water and zero for the body and the air. Red=1.Blue=0.

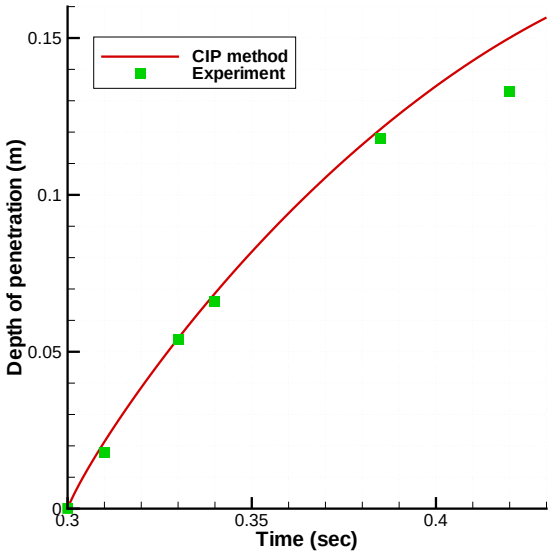

Fig. 16 Depth of penetration during water entry of a half-buoyant cylinder

Figure 17 shows the free surface deformation of a neutrally buoyant cylinder at several time instants. Similar to the half buoyant cylinder, after the cylinder reaches the free surface, two jets are thrown up on both sides of the cylinder and move away from the cylinder, leaving the upper part of the cylinder dry even when h/R>2. The free surfaces on the two sides of the air cavity eventually become unstable and the cavity formed behind the cylinder collapses. The free surfaces of the open air cavity above the cylinder impact first against each other at the cylinder surface. The impact throws up another jet. Some air bubbles can be seen along the cylinder moving upwards to the free surface.

At t=0.50s, the cylinder reaches the bottom of the tank and bounces up. Since the bottom of the tank is not modeled in this computation, we made the same treatment as Xing-Kaeding et al. (2004), i.e. the velocity of the cylinder is simply reversed at this time instant to simulate a loss-free re-bounce.

Figure 18 shows the time history of the penetration depth of the neutrally buoyant cylinder. At t=0.34s, the experimental data is clearly larger than the numerical result. However, Greenhow & Lin (1983) put a question mark over this point.

Figure 17 and 18 show in general satisfactory agreement between the numerical results and experimental data for the neutrally buoyant cylinder.

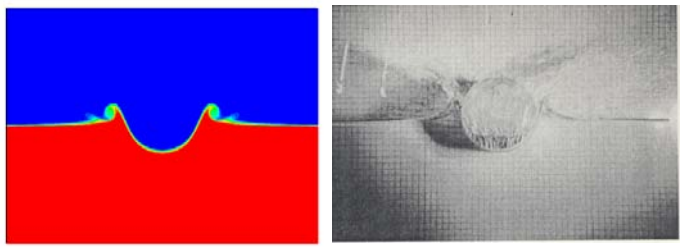

t=0.315s

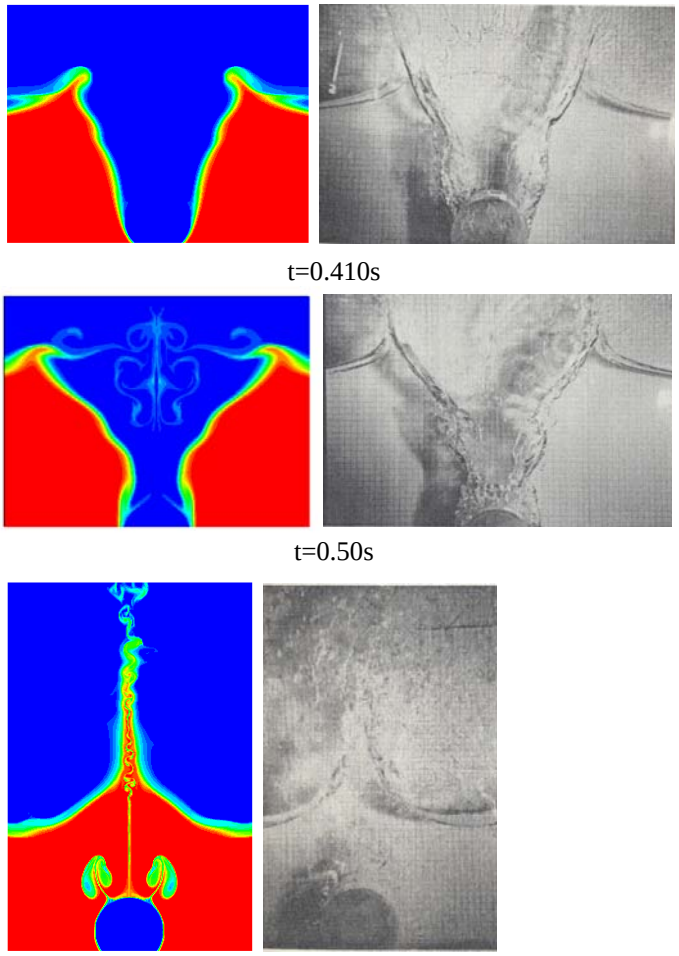

t=0.410s

t=0.50s

t=0.75s

Fig.17 Free surface deformation during water entry of a neutrally buoyant cylinder. CIP simulations (left) and experiments by Greenhow & Lin (right). The CIP calculations show the density function φ_1 which is theoretically one for water and zero for the body and the air. Red =1. Blue=0.

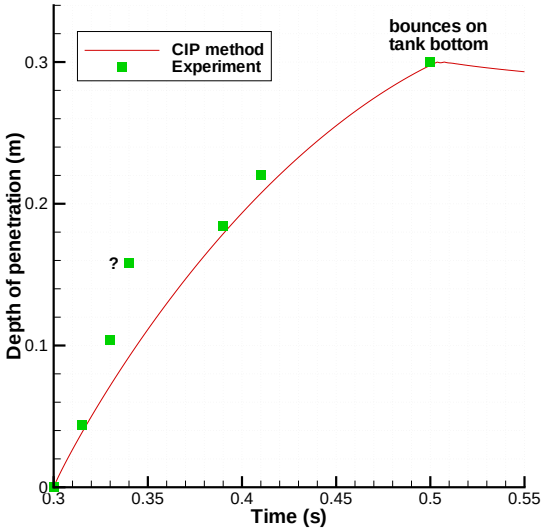

Fig. 18 Depth of penetration during water entry of a neutrally buoyant cylinder

Water exit with constant force

We study now a neutrally buoyant cylinder that rests on the tank bottom and is lifted by applying a constant force equal to the cylinder weight. Numerical results are compared with the experiments conducted by Greenhow & Lin (1983).

Figure 19 shows the free surface deformation at several time instants. The numerical simulations predicted the dominating phenomena during the water-exit of a cylinder: the water above the cylinder is lifted by the cylinder and thin layers of water are formed subsequently on the top of the cylinder. When the cylinder further rises up, the thin water layer is drawn down along the cylinder and causes the breaking of the free surface. The fact that viscous flow separation has occurred (see Fig. 13) lowers the pressure below the cylinder. The numerically predicted pressure distribution at time instant t=0.248s is illustrated in Fig. 20. Since the total pressure in the water is clearly higher than the vapor pressure (e.g. 2336.9Pa at 20°C). cavitation does not occur. However, the predicted pressure in the water is lower than the atmospheric pressure in the vicinity of the free surface below the cylinder. This suggests that ventilation happens and is confirmed by the experimental results showing a mixture of the water and the air below the cylinder. The numerical simulations in Fig. 19 show two large eddies below the cylinder with a yellow-like color. This color implies a mixture between the water and the air. However, the fine details of how ventilation occurs require further studies. Moyo & Greenhow (2000) associate the break-down of the free surface and resultant ventilation with the fundamental fluid-mixing mechanism connected with the Rayleigh-Taylor instability. This occurs when a light fluid (e.g. air) is accelerated into a heavy fluid (e.g. water).

Figure 21 shows the distance from the cylinder top to the mean free surface. From these figures, we can see that the simulations and experiment agree well.

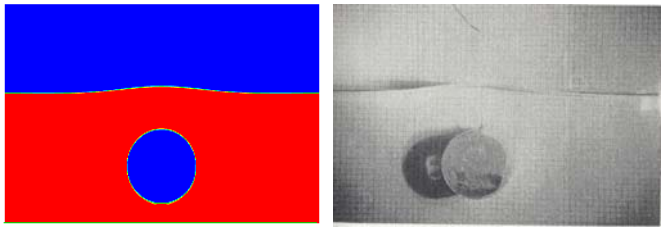

t=0.072s

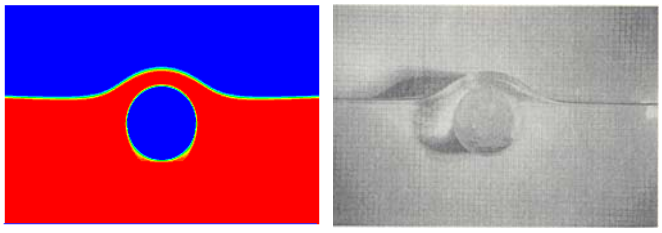

t=0.165s

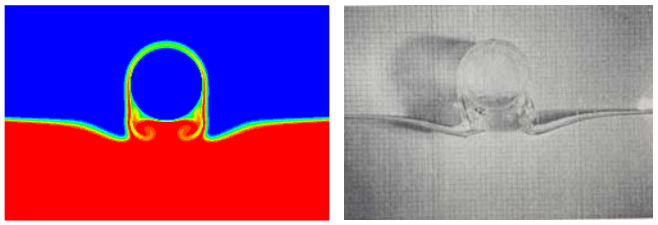

t=0.220s

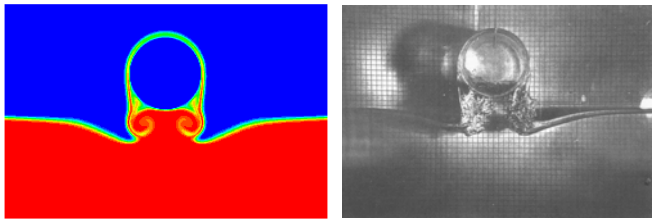

t=0.248s

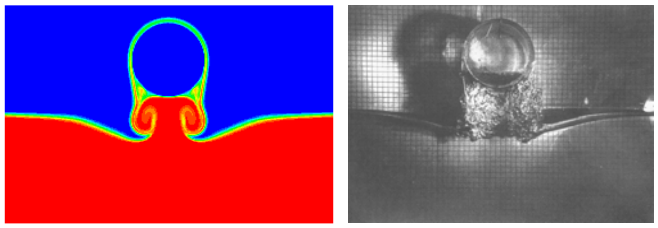

t=0.280s

Fig. 19 Free surface deformation during water exit of a neutrally buoyant cylinder. CIP simulations (left) and experiments by Greenhow & Lin (right). The CIP calculations show the density function φ_1 which is theoretically one for water and zero for the body and the air. Red=1. Blue=0

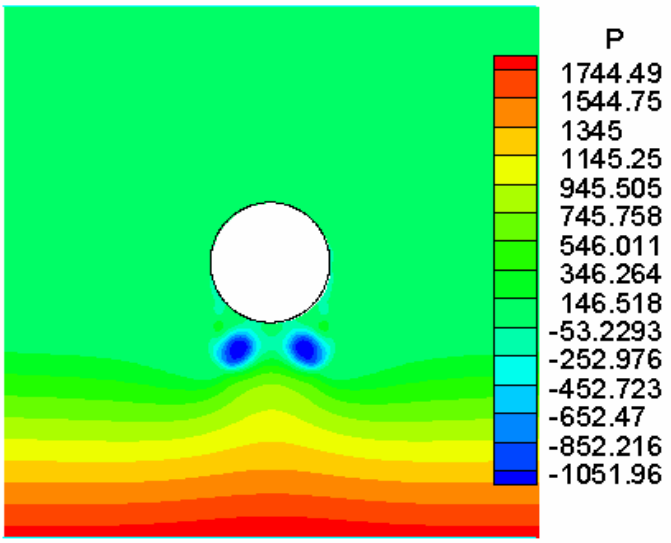

Fig. 20 Predicted pressure distribution in Pascal at t=0.248s for the water exit described in Fig. 19. The atmospheric pressure has to be added to obtain the total pressure.

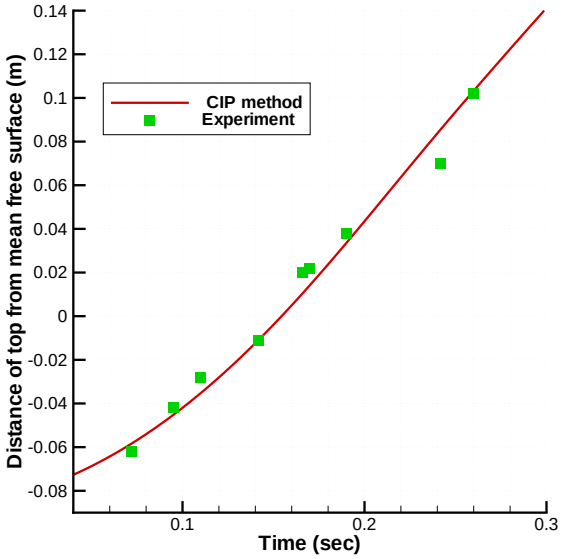

Fig. 21 Distance from the cylinder top to mean free surface during water exit of a neutrally buoyant cylinder

CONCLUSIONS

This paper presents numerical simulations of water-entry and water-exit of a circular cylinder with both forced and free vertical motions by using a CIP-based finite difference method. The circular cylinder and free surface interaction is treated as a multiphase problem, while the free surface as well as the body boundary is immersed in the computational domain. One set of governing equations is used to represent the motion of different phases, and these equations are solved numerically on a non-uniform, staggered Cartesian grid by a finite difference method.

The CIP calculations give a good overall agreement with the experiments by Miao (1989) for water entry and water exit with constant velocity. Non-viscous flow separation and wave generation are important factors during water entry after an initial penetration phase. Viscous effects have a minor influence on the water entry force.

The predicted vorticity associated with viscous flow separation, the time rate of change of kinetic fluid energy and the free surface deformation give a reasonable explanation of the phenomena observed during water exit.

The complicated free surface deformation is simulated with good agreement to the photographs taken from the experiments conducted by Greenhow & Lin (1983). The motion of the cylinder for both water entry and water exit agrees also well with the experimental data.

These studies demonstrate that the CIP-based method is applicable to the water-entry and water-exit problems.

ACKNOWLEDGMENTS

This work is supported by the BeMatA project sponsored by the Norwegian Research Council. The comments by M. Greenhow are appreciated.

REFERENCES

Campbell, I. M. C. & Weynberg, P. A. (1980) Measurement of parameters affecting slamming. Final Report, Rep. No. 440, *Technology Reports Center No. OT-R-8042*. Southampton University: Wolfson Unit for Marine Technology.

Chezhian, M. (2003) Three-dimensional analysis of slamming. Dr.ing thesis. Dept. of Marine Technology, NTNU, Trondheim, Norway.

Faltinsen, O. M. (1990) *Sea Loads on Ships and Offshore Structures*. Cambridge, England: Cambridge University Press.

Faltinsen, O. M. (2005) *Hydrodynamics of High-Speed Marine Vehicles.* New York: Cambridge University Press.

Greenhow, M. & Lin, W.M. (1983) Nonlinear free-surface effects: experiments and theory. Report, MIT, Department of Ocean Engineering, pp. 83-119.

Hu, C.-H & Kashiwagi, M. (2004) A CIP method for numerical simulation of violent free surface flows. *J. Mar Sci Tecnol.* **9**, pp. 143-157.

Miao, G. (1989) Hydrodynamic forces and dynamic responses of circular cylinders in wave zones. Dr.ing thesis, Dept. of Marine Hydrodynamics, NTH,Trondheim.

Moyo, S. & Greenhow, M. (2000) Free motion of a cylinder moving below and through a free surface. Applied Ocean Research **22** (2000) 31-44.

Sarpkaya, T. (1966) Separated flow about lifting bodies and impulsive flow about cylinders, *AIAA Jour*., **44**, 414-20.

Schlichting, H. (1979) *Boundary-Layer Theory*. New York: McGraw-Hill Book Company.

Sun, H. (2004) Solution of exercises in the book "*Hydrodynamics of High-Speed Marine Vehicles*" by Prof. O. Faltinsen, Centre for Ships and Ocean Structures, NTNU, Trondheim, Norway.

Wagner, H. (1932) Über Stoss- und Gleitvorgänge an der Oberfläche von Flüssigkeiten. *Zeitschr. f. Angewandte Mathematik und Mechanik,* **12**, 4, pp. 193-235.

Walton, P. (1986) Ph.D. thesis. University of Manchester.

White, F. M. (1974) *Viscous Fluid Flow*. New York: McGraw-Hill Book Company.

Xing-Kaeding, Y., Jensen, G. & Peric, M. (2004) Numerical simulation of water-entry and water-exit of a horizontal circular cylinder. Hydrodynamics VI - Theory and Application, A. A. Balkema Publisher, pp. 663-669.

Zhao, R. & Faltinsen, O. (1993) Water-entry of two-dimensional bodies. *J. Fluid Mech*. **246**, pp. 593-612.